Study to Improve Thermoelectric Properties by Doping Mechanism using $CsBi_4Te_6$ and Half Heusler Bulk Materials

Arun Kumar[1], Tarun gupta[2], Vinod seharawat[3], Nitin kumar[4], Susheel Kumar Upadhyay[5] and Girish Dutt Gautam[6]

[1,2,3,4]NGFCET Palwal
[5]BSACET Mathura
[6]JayPee University of Information Technology, Samirpur, Hamirpur (HP)

Abstract—*Thermoelectric (Peltier) heat pumps are capable of refrigerating solid or fluid objects, and unlike conventional vapor compressor systems, they can be miniaturized without loss of efficiency. More efficient thermoelectric materials need to be identified, especially for low-temperature applications in electronics and devices. The material CsBi4Te6 has been synthesized and its properties have been studied. When doped appropriately, it exhibits a high thermoelectric Fig. of merit below room temperature (ZT_{max}: 0.8 at 225 kelvin). At cryogenic temperatures, the thermoelectric properties of CsBi4Te6 appear to match or exceed those of Bi2ÐxSbxTe3ÐySey alloys. Moreover, nano composite approaches have been used to study the thermoelectric properties of other material systems such as CsBi4Te6 and half-Heusler phases. We observed a significant improvement in peak ZT of nano structured n-type HH compound 0.8 to 1.0 respectively. Here we studied only n-type HH compounds. The improvement of Fig. of merit is mainly due to the reduction of thermal conductivity. This nanostructure approach is applicable to many other thermoelectric materials that are useful for automotive, industrial waste heat recovery, space power generation and many other fields.*

1. INTRODUCTION

As the increasing demand for energy rapidly, it is becoming more important to develop new, inexpensive materials that can supply sustainable and clean energy to meet the needs of the future.

The phenomenon **Thermoelectric** was discovered more than 180 years ago. But now a day it is a very interesting topic in research for clean energy. This phenomenon introduce by German scientist Thomas Johann **Seebeck** (1770-1831), who was born in the Estonian town Revel. Seebeck discovered that if the ends of two heterogeneous metals soldered at two junctions (hot junction and cold junction) under different temperature (T and T+ΔT) conditions were closed. Than a voltage difference (ΔV) developed that was directly proportional to the temperature difference. This phenomenon is referred to as the Seebeck's effect.

This effect can be used to generate electricity, measure temperature or change the temperature of objects. Because the direction of heating and cooling is determined by the polarity of the applied voltage, thermoelectric devices can be used as temperature controllers.

Thermoelectric effect- The term "thermoelectric effect" encloses three separately identified effects: the Seebeck effect, Peltier effect, and Thomson effect. In this paper, I only focus on the Seebeck effect.

Seebeck effect- When two ends of a conductor are held at different temperatures, electrons at the hot junction at higher thermal velocities diffuse to the cold junction. Seebeck discovered that making one end of a metal bar hotter or colder than the other produced an EMF between the two ends. The ratio of the voltage developed to the temperature gradient (ΔV/ΔT) is related to an intrinsic property of the materials called the Seebeck coefficient or the thermo power.

$$\Delta V = S \Delta T$$

2. THERMAL AND ELECTRICAL TRANSPORT PROPERTIES

Seebeck coefficient

Again from Boltzmann's equation, a general expression for the Seebeck coefficient can be

Fig. 1-Seebeck effect

written as

$$S = \frac{1}{eT} \frac{\int \sigma (E - E_F) dE}{\int \sigma (E) dE} \alpha (E - E_F)$$

From equation 1.2.5, it is clearly seen that the Seebeck coefficient is proportional to the expectation value of energy difference of the carriers and Fermi energy. This relationship

 ISBN: 978-81-930585-9-6

could prove useful to engineer a material such that low energy carriers are cut off and a higher Seebeck coefficient could be observed.

Electrical conductivity

Electrical conductivity is the property of a material that indicates its ability to conduct current. From Boltzmann's transport

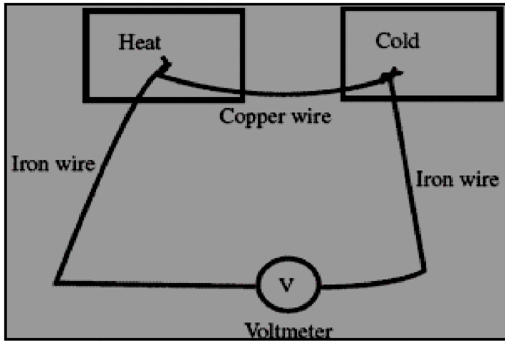

Fig. 1: Seebeck effect

equation, a general expression for electrical conductivity can be calculated as

$$\vec{\sigma} = -\frac{e^2}{4\pi^3}\int \tau \vec{v}(\vec{\kappa})\vec{v}(\vec{\kappa})\frac{\partial f_0}{\partial E} d^3K$$

Where $\vec{\sigma}$ a symmetric second rank conductivity tensor, τ is relaxation time, $\vec{v}(\vec{k})$ is velocity of carriers, and f_0 is distribution function. The evaluation of the integral in equation 1.2.1 over all k-space depends on the relations of $E(\vec{k})$ with $\vec{v}\vec{v}$ terms, and the temperature dependence of σ comes from the $\frac{\partial f_0}{\partial E}$ For semiconductors, electrical conductivity can be evaluated by using the Fermi function as the distribution function and an isotropic, parabolic energy band. With these approximations, electrical conductivity can be written as,

$$\sigma = \frac{2e^2\tau}{m^*}\left(\frac{m^* k_B T}{2\pi\hbar^2}\right)^{3/2} \exp(-|E_F|/K_B T$$

Thermal conductivity

Thermal conductivity is the property of a material that indicates its ability to conduct heat. Thermal conductivity is measured in SI units of $Wm^{-1}k^{-1}$.Thermal conductivity in thermoelectric mainly comes from (1) electrons and holes transporting heat (k_e) and (2) phonons travelling through the lattice (k_l), (k_e)and σ are directly related through the Wiedemann-Franz law:

$$k_e = L \sigma T$$

Where k_e is electrical thermal conductivity, L is the Lorenz factor, 2.4×10-8 $J^2K^{-2}C^{-2}$ for free electrons, σ is electrical conductivity, and T is temperature. Electrical thermal conductivity is sensitive to carrier concentration and carrier mobility. As carrier concentration increases, the electrical thermal conductivity increases linearly.

The Fig. of Merit-

The seebeck coefficient, Electrical and thermal conductivity of a material are summarized in the so called "Fig. of merit" of a thermoelectric material, usually written"ZT". The Fig. of merit *(ZT)* is expressed as

$$ZT = \frac{\sigma S^2 T}{\lambda}$$

Where σ =1/ρ is electrical conductivity, K is thermal conductivity, T is temperature, and ρ is electrical resistivity.

The output of a thermoelectric generator is related to the power factor, $s^2\sigma$. Because the ZT of a material depends on temperature, materials are chosen for specific applications to maximize ZT. According to the formulae $ZT = \frac{\sigma S^2 T}{\lambda}$, the materials suitable for thermoelectric application with good thermoelectric performance meet the following: (1) the materials should have high thermal conductivity; (2) low thermal conductivity; and (3) high thermal power or seebeck coefficient Goupil C [3]. Metals are good electrical conductor with high charge concentration. Thermocouple based on the thermoelectric effect in metals. However, metals are also having high thermal conductivity, which causes a low Fig. of merit, ZT Dresselhaus, M. et al. Adv. Mater [2]. Therefore, metals cannot be used for power generation. Most insulator have low thermal conductivity (except for Sic, diamonds, etc.), but they do not conduct electricity at all. Therefore, semiconductor should be good thermoelectric material. Semiconductor should have lower thermal conductivity than metals, although they also have lower electrical conductivity than metals Herman's, J. P., [5].

Thermal power is inversely proportional to the charge concentration. Semiconductors have less charge concentration than metals. Semiconductors have large thermal power compared to metals. Maximizing electric conductivity and minimizing thermal conductivity in semiconductors can achieve the maximum Fig. of merit. Therefore, all thermoelectric materials with good thermoelectric properties that have been discovered and widely studied so far are based on semiconductors. They can be divided into several groups: tellurium-based, antimony-based, and silicon-based semiconductor compounds. Tellurium-based compounds are useful for low and room temperature application, while antimony developed by the National aeronautics and space Administration (NASA) for thermoelectric power generation:

(a) p-type and (b) n-type. Most of these materials are complex alloy with dopants. Developing thermoelectric materials with superior performance means tailoring interrelated thermo-electric physical parameters electrical conductivities, Seebeck coefficients, and thermal conductivities–for a crystalline system. High electrical conductivity, low thermal conductivity, and a high Seebeck coefficient are desirable for thermoelectric materials. Therefore, knowledge of the relation between electrical conductivity and thermal conductivity is essential to improve thermoelectric properties. In general, research in recent years has focused on developing thermoelectric structures and materials of high efficiency Koumoto K [4]. The importance of this parameter is universally recognized; it is an established, ubiquitous, routinely used tool for material, device, equipment and process characterization both in the thermoelectric industry and in research. In this paper, basic knowledge of thermoelectric materials and an overview of parameters that affect the Fig. of merit ZT are provided. The prospects for the optimization of thermoelectric materials and their applications are also discussed

Doping mechanism in CsBi4Te6

A broad search is under way to identify new materials with enhanced thermoelectric (TE) properties [7–9]. Important applications include cooling of electronic circuitry and superconducting devices. Particularly desirable are candidate materials that function well at or below room temperature, with performance characteristics better than those of the well-known Bi22xSbxTe32ySey alloys. We have explored materials with more complex compositions and structures that would likely have complex electronic structures that could give rise to high TE performance. Good TE materials require an unusual combination of electrical and thermal properties. The challenge lies in achieving simultaneously high electrical conductivities, high TE power S, and low thermal conductivity k, which define the unit less TE Fig. of merit ZT 5 (S2s/k)T (where T is temperature). All three of these properties are determined by the details of the electronic structure (band gap, band shape, and band degeneracy near the Fermi level) and scattering of charge carriers (electrons or holes) and thus are not independent. The total thermal conductivity k also has a contribution from the phonon thermal conductivity, kl, such that k 5 ke 1 kl, where ke is the carrier thermal conductivity. Recently we reported that K2Bi8S13 and b-K2Bi8Se1 have promising TE properties and particularly low k values. The alkali metals play an important role in reducing the total k. When we moved on to investigate corresponding Te analogs with Cs, we obtained an unexpected result: Instead of Cs2Bi8Te13, we isolated CsBi4Te6. From a chemical point of view, this amounts to a reduction of a Bi2Te3 unit by a half-equivalent of electrons. The added electrons, however, result in a complete restructuring of the Bi2Te3 framework so that the new structure bears no resemblance to the corresponding binary compound. The new compound seems to be an outstanding candidate for low-temperature TE applications. We describe here the synthesis, structure, and TE properties of CsBi4Te6, which, when doped appropriately, achieves a maximum ZT of ;0.8 at 225 K, making it the best bulk TE material below room temperature. We first obtained CsBi4Te6 by reacting Cs2Te and Bi2Te3 at 700°C. Subsequently we devised a synthesis from the direct stoichiometric combination of the elements at 600°C. The material is stable in air and water, and melts without decomposition at 545°C. The crystals grow with long needle-like morphology. The direction of rapid growth along the needle axis is also the direction of maximum TE performance. CsBi4Te6 has a layered anisotropic structure. It is composed of anionic [Bi4Te6] slabs alternating with layers of Cs1 ions. The addition of one electron per two equivalents of Bi2Te3 is not top tactic and does not produce a formal intercalation compound, but causes a complete reorganization of the bismuth telluride framework to produce a new structure type. The added electrons localize on the Bi atoms to form Bi-Bi bonds that are 3.238 6 0.001 Å long. The presence of these bonds is unusual in bismuth chalcogenide chemistry, and it is not clear whether they play a role in the enhanced TE properties of the material. The [Bi4Te6] layers are strongly anisotropic, as they consist of one-dimensional (1D) [Bi4Te6] lathlike ribbons running parallel to the b axis. The width and height of these laths is 23 Å by 12 Å. The laths arrange side by side and are connected via the Bi-Bi bonds mentioned above. This structural feature is responsible for the strongly 1D needle-like appearance of the CsBi4Te6 crystals. The Bi atoms are octahedral surrounded either by six Te atoms or by five Te atoms and one other Bi atom. The degree of distortion around the Bi atoms is relatively small. The longest and shortest Bi-Te bonds are 3.403 6 0.001 Å and 2.974 6 0.001 Å, respectively, with an average distance of 3.18 Å. The Cs1 ions lie between the layers, and their atomic displacement parameters are 1.6 times those of the Bi and Te atoms, which suggest that they undergo considerable “rattling” motion. Such a dynamic motion in the lattice can be responsible for strong scattering of heat-carrying phonons and leads to low k values. The immediate environment of Cs is a square prismatic arrangement of Te atoms. As obtained directly from the synthesis (with no deliberate attempt at doping), crystals of CsBi4Te6 have high room-temperature s values, ranging from 900 to 2500 S/cm (20), and S values from 90 to 120 mV/K (21). At lower temperatures, S typically exhibits a maximum of 120 mV/K at; 240 K and then slopes toward zero at 0 K. The k measurements on a large number of pressed pellets (.97% theoretical density) or oriented ingots (22) show values between 1.25 and 1.85 W/mzK, for lightly and heavily doped samples, respectively. These values give rise to relatively high room-temperature ZT values of 0.2 to 0.5; these Fig. s of merit suggest that the material is an excellent candidate for further optimization via chemical manipulation (such as doping, solid solution, and crystal growth). On the basis of the maximum values of S, the band gap of CsBi4Te6 can be estimated from the formula E.g. $2S_{max}ZT_{max}$ to be between 0.05 and 0.11 eV. Because of the promising properties of CsBi4Te6, we pursued

doping studies of this material with various chemical doping agents. We investigated SbI3, BiI3, and In2Te3 in amounts varying from 0.02 to 4 mole percent. These dopants were chosen for the purpose of placing halide atoms in the Te 1Department of Chemistry, Michigan State University and Center for Fundamental Materials Research, East Lansing, MI 48824, USA. 2Electrical and Computer Engineering & Materials Science and Mechanics, Michigan State University, East Lansing, MI 48824, USA. 3Department of Electrical Engineering and Computer Science, Northwestern University, Evanston, IL 60208, USA 4Department of Physics, University of Michigan, Ann Arbor, MI 48109, USA. Doping with these agents does occur, but we currently do not know what sites in the crystal structure are being occupied. Surprisingly, doping with SbI3 and BiI3 produces *p*-doped rather than *n*-doped samples. This observation is not consistent with iodine atoms occupying Te sites but instead suggests Sb and Bi atoms on Te sites. The Sb and Bi atoms, having only five electrons, introduce holes in the Te-based valence band. However, In2Te3 can produce *n*-type samples (see below). Depending on the type and degree of doping, room-temperature *S* values between 1175 mV/K and100 mV/K were observed. CsBi4Te6 is amenable to considerable doping manipulation, much like Bi2Te3, and thus higher ZT values may be obtainable. The s and *S* data were used to calculate the power factors, *S*2s, for each dopant versus temperature and doping concentration. The best results in this study were obtained with SbI3. The evolution of power factor as a function of SbI3 addition is shown in Fig. 3A. From these data, the optimal concentration seems to lie at 0.05% SbI3. This sample achieved a maximum power factor of; 51.5 mW/cmzK2 at 184 K. The temperature dependences of s and *S* of the best sample are shown in Fig. 3B The *S* maximum was found at ;250 K. The total k of the doped samples of the material,;1.48 W/mzK (Fig. 3C) (*24*), is considerably smaller than that of Bi2Te3 (at;1.85 W/mzK) and more comparable to that of the optimized Bi22*x*Sb*x*Te3–*y*Se*y* alloy (at 1.56 W/mzK). The approximate electronic contribution to k was estimated using the Wiedemann-Franz law for metals as ke ; 0.7 W/mzK. This result suggests that the measured total k of this material is almost equally composed of the lattice and electronic contributions. Perpendicular to the growth axis (*b* axis), k was sharply lower (;0.6 W/mzK), which reflects the highly anisotropic nature of CsBi4Te6. The ZT for this sample (0.05% SbI3- doped CsBi4Te6) and that of the optimized commercial Bi22*x*Sb*x*Te3 are compared as a function of temperature. Along the growth axis, the computed ZT values for CsBi4Te6 reach a maximum of 0.82 at 225 K and 0.65 at room temperature. In contrast, optimized Bi22*x*Sb*x*Te3 *p*-type alloy has a peak of ZT; 0.95 at room temperature, whereas at 225 K, its ZT drops to 0.58. Both ZT curves are similar in shape, but that of CsBi4Te6 is shifted (by; 70 K) to lower temperatures. Because the CsBi4Te6 samples reach optimum performance at a much lower temperature than does Bi22*x*Sb*x*Te3, we expect that this new material could be exploited for low-temperature applications, particularly in the temperature range where Bi22*x*Sb*x*Te3 alloy is ineffective. Recent optimization work on *p*-type Bi22*x*Sb*x*Te32*y*Se*y* alloys claimed low-temperature (; 210 K) ZT_{max} values of 0.64 Preliminary Hall-effect measurements for SbI3-doped CsBi4Te6 samples show that carrier concentrations are on the order of 3 3 1018 to 1019 cm23 for samples doped at 0.1% and 0.2% SbI3. Hole motilities calculated from the electrical conductivity and Hall data show exponentially decreasing mobility as the temperature increases. These are substantially greater than those typically found in the optimized *p*-type bismuth telluride alloy (; 380 cm2/Vzs) (*28*). At low temperatures, the mobility soars to 5000 cm2/Vzs. The very high whole mobility could be due to the 1D character of CsBi4Te6 and the lack of atomic disorder in its crystal lattice. The carrier concentration shows a weak dependence on temperature, with values decreasing as the temperature is lowered. The carrier concentration tends to diminish as the doping increases away from 0.05% SbI3, the material with the highest power factor. For these samples, the carrier concentration data could be correlated with the power factor data; the results showed that the power factor decreased as the carrier concentration moved away from 1019 cm23 A complete TE cooling device needs both a *p*-type and an *n*-type version of a material to operate. Thus, an important issue to be addressed in future studies with CsBi4Te6 is whether *n*-type doping is possible. We have been able to show that In2Te3 doping leads to *n*-type charge transport. Not only is *n*-type behavior achievable, but the maximum TE power of 2100 mV/K occurs at;160 K, a temperature with important implications for the development of even lower temperature TEs. Although optimum levels have not yet been reached, we believe additional improvements in TE performance in this material are possible with further exploration of doping agents and the investigation of solid solutions such as CsBi42*x*Sb*x*Te6, CsBi4Te62*x*Se*x*, and Cs12*x*Rb*x*Bi4Te6. The latter could result in substantially lower thermal conductivities (as much as 30 to 50% lower), giving projected values of ZT. 1.5. Band structure calculations for CsBi4Te6 should provide further insight into the electronic properties of this material.

Doping Mechanism in HH compound

Heusler and half-heusler phases are respectively represented by the general structures ' 2 *M MX* and *MM*'X, where *M* and *M*' are metals, and X is a *sp* metalloid or metal. For a majority of the Heusler phases, *M*' is either a transition metal or noble metal, and *M* is a transition metal, a noble metal, or a rare-earth metal. The crystal structure of the heusler phase is of the Bi3F type (space group Fm3m) and its unit cell consists of four interpenetrating face-centered cubic (FCC) sublattices.

Each of the four FCC sublattices has the same unit cell size as that of the heusler phase. In one unit there are 16 atoms. Two of the FCC sublattices, denoted by *MX*, form a rock-salt substructure. The other two FCC sublattices, denoted by ' 2 *M,* occupy equivalent sites (0, 0, 0) and (½, ½, ½). The rock-salt substructure *MX* and fcc sublattices ' 2 *M* are mutually displaced with respect to each other along their body diagonals

by one-quarter of the unit cell. With each of the cubic interstices of *MX* being filled by an *M*' atom, the Heusler phase can be described as a “stuffed rock salt”. If one of the ' 2 *M* sublattices is vacant, the half-Heusler phase (space group F43m, MgAgAs-type) is formed. The latter phase, which is now a “half-stuffed rock salt,” has 12 atoms per unit cell (Fig. 6.2.1). A typical X-ray pattern of half-Heusler phases has been published in literature[12], which resemble a face-centered cubic lattice for these compounds which means all hkl’s are either odd or even Both Heusler and half-Heusler phases are chemically diverse and known to exist in more than 350 and 140 alloy systems, respectively.

HH samples are prepared by a dc hot press of ball milled powder of an ingot which is initially made by Arc melting process. In Arc melting furnace where a required composition of n-type half-Heusler compounds are melted to get ingots. Then the melted ingots are ball milled for 5 – 20 hours to get the desired alloyed nanopowders. The mechanically prepared nanopowders are then pressed at temperatures of 1000 – 1050^0C b using a dc hot press method in graphite die with a 12.7 mm central cylindrical opening diameter to get bulk nanostructured half-Heusler samples. The samples were characterized by X-ray diffraction (XRD), Scanning electron microscopy (SEM) and Transmission electron microscopy (TEM) to study their crystallinity, composition, homogeneity, average grain size, and grain size distribution of the nano particles. These parameters significantly affect the thermoelectric properties of the final dense bulk samples. The volume mass densities of these samples were measure using an Archimedes’ kit.

These parameters significantly affect the thermoelectric properties of the final dense bulk samples. The volume mass densities of these samples were measure using an Archimedes’ kit.

In this section, we discuss the results for the thermoelectric properties of n-type half-Heusler phases of compositions $Hf_{0.75}Zr_{0.25}$ $NiSn_{1-x}Sb_x$ where x=0.025, 0.01, 0.005. Fig. 7 shows the XRD pattern (a) and SEM images (b-c) of the arc melted and ball milled $Hf_{0.75}Zr_{0.25}NiSn_{0.99}Sb_{0.01}$(x=0.01) sample. The pattern from XRD (Fig.7) is matched with those obtained for half-Heusler phases [13] showing the quality of the sample for better thermoelectric properties.

Fig. s7b & c clearly show the sample from the ball milled and hot-pressed contains particles having sizes of few hundred nanometers to several micrometers. The sample from the ball milled and hot-pressed are significantly smaller in comparison to that of arc melted samples [13] which is favorable for the lower thermal conductivity due to possible increase in phonon scattering.

Fig. s8 show the temperature dependent electrical conductivity (a), Seebeck coefficient (b), power factor (c), thermal conductivity (d), and ZT (e) of nanostructured HH samples of compositions $Hf_{0.75}Zr_{0.25}NiSn_{1-x}Sb_x$ where x=0.025, 0.01, 0.005. Fig. s 8a and b clearly show that if the antimony doping will decrease than the electrical resistivity and Seebeck coefficient both increase. This could be due to a decrease of carrier concentration. As a result, the optimized power factor for $Hf_{0.75}Zr_{0.25}NiSn_{0.99}Sb_{0.01}$(x=0.01) sample is observed (Fig.8c). Moreover, Fig. 8d shows that the thermal conductivity also decreases with decreasing the antimony doping, which is also an effect of carrier concentration, giving maximum value of ZT is 1.0 at 700°C in nanostructured sample at x=0.01 composition (Fig.8e), which is about 20 % improvement in comparison to the previously reported maximum value of ZT [14]. Fig. 8 show the temperature dependent electrical conductivity (a), Seebeck coefficient (b), power factor (c), thermal conductivity (d), and ZT (e) of nanostructured at x=0.01 sample in comparison to a reference sample. The reference sample is prepared from arc melting $Hf_{0.75}Zr_{0.25}NiSn_{0.975}Sb_{0.025}$(x=0.025) composition, which has the best ZT values so far [14]. Fig. s 8a and b clearly show that the electrical resistivity and Seebeck coefficient of the nanostructured sample is much higher in comparison to the reference sample giving a little bit higher power factor (Fig. 6.4.3c). There could be two reasons behind this effect.

1 The carrier concentration decrease in nanostructured samples since it has lower antimony doping, and

2 The mobility decrease in nanostructured sample due to the creation of defects by ball milling.

However, the thermal conductivity of the reference sample is significantly higher in comparison to the nanostructured sample (Fig. 8d). The reasons of lower thermal conductivity in the nanostructured sample could be due to lower carrier contribution and increased phonon scattering through grain boundaries of nanostructures. As a result, a peak ZT of 1.0 is observed in the n-type nanostructured $Hf_{0.75}Zr_{0.25}NiSn_{0.99}$ $Sb_{0.01}$ sample, which is about 20 % improvement in comparison to the reference sample (Fig. 8e). This ZT improvement mainly comes from the reduction of thermal conductivity in the nanostructured sample due to increased phonon scattering through the grain boundaries of nanostructures, and the increase in power factor due to optimization of carrier concentration by antimony doping.

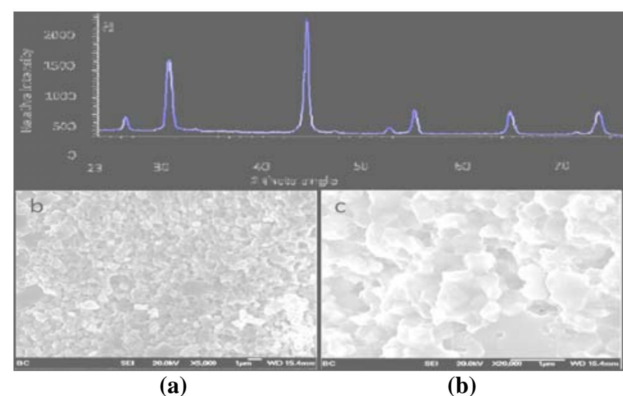

(a) (b)

 ISBN: 978-81-930585-9-6

Fig. 7: XRD pattern (a) and SEM images (b-c) of arc melted and ball milled $Hf_{0.75}Zr_{0.25}NiSn_{0.99}Sb_{0.01}$ sample.

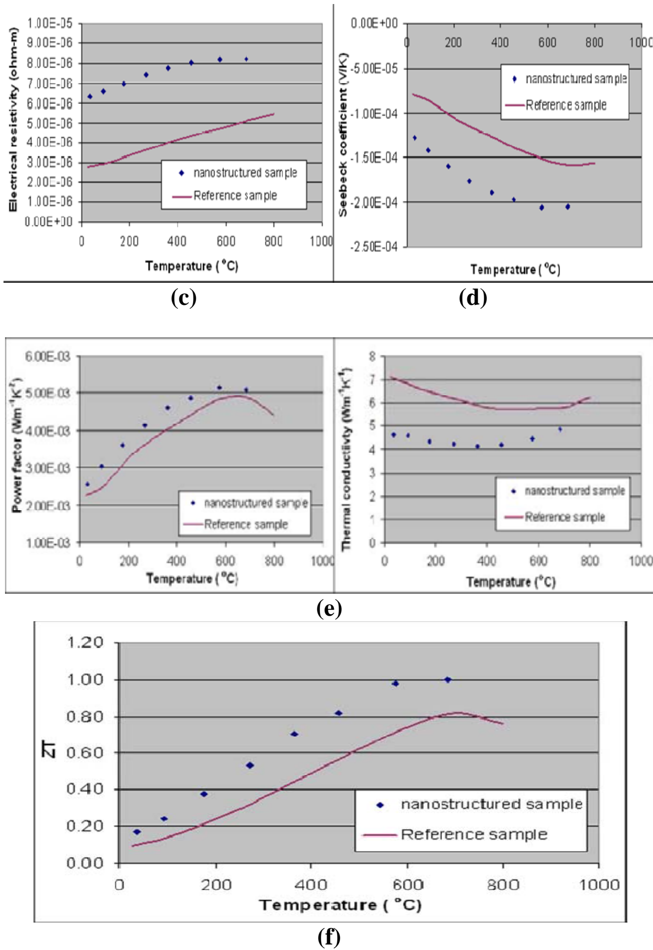

Fig. 8: Temperature dependent electrical conductivity (a), Seebeck coefficient (b), power factor (c), thermal conductivity (d), and ZT (e) of nanostructuredHf0.75Zr0.25NiSn0.99Sb0.01sample in comparison to a reference sample..

3. CONCLUSION

In recent years, many studies have shown a significant enhancement of ZT in other material systems via nanostructuring approach to reduce the thermal conductivity by scattering phonons more effectively than electrons at interfaces in super lattices and in bulk materials, such as lead antimony silver telluride (LAST) alloys, and skutterudites with an operating temperature up to 600^0C. We have been pursuing for applications at around 1000^0C, such as for radio-isotope thermoelectric generators (RTGs) used in space missions, The ZT enhancement is due to a large reduction in the thermal conductivity while maintaining the electron transport properties material by increasing the power factor. Moreover, a modulation doping technique is applied in ZnO alloys to improve the power factor by increasing the mobility. The increase in mobility is due to reduced ionized and unionized impurity scattering by spatial separation of doped carriers. Some of the points show that increasing Fig. of merit of ZnO and HH material with doping mechanism.

1) For CsBi4Te6 samples, the electrical conductivity and Seebeck coefficient increased with increasing temperature. As a result the power factor is increase. At 1173K, the highest power factor of ~9.31×10^{-4} $Wm^{-1}K^{-2}$ measured. Moreover, the thermal conductivity rapidly decreases with increase in temperature.
2) The electrical conductivity and Seebeck coefficient both increase with decreasing the antimony doping. This could be due to a decrease of carrier concentration with decreasing antimony doping. As a result, the optimized power factor is increase. Moreover, the thermal conductivity also decreases with decreasing the antimony doping, which is also an effect of carrier concentration, giving peak ZT of 1.0 at 700°C in nanostructured sample of $Hf_{0.75}Zr_{0.25}NiSn_{0.99}Sb_{0.01}$ composition, which is about 20 % improvement in comparison to the previously reported peak ZT value.

REFERENCES

[1] Bubnova O, Khan ZU, Malti A, Braun S, Fahlman M, Berggren M, et al. Optimization of the thermoelectric Fig. of merit in the conducting polymer poly(3,4-ethylenedioxythiophene). Nat Mater 2011; 10:429–33.
[2] Dresselhaus, M. et al. Adv. Mater.2001, 19, 1.
[3] Goupil C, Seifert W, Zabrocki K, Muller E, Snyder GJ.Thermodynamics of Thermoelectric Phenomena and Applications. Entropy 2011; 13:1481–517.
[4] Koumoto K, Wang Y, Zhang R, Kosuga A, Funahashi R. Oxide Thermoelectric Materials: A Nanostructuring Approach. Annu Rev Mater Res 2010; 40:363–94.
[5] Nolas, G. S. et al. J. Appl. Phys. 1996, 79, 4002.
[6] Rowe, D. M., and Bunce, R. W. J.
[7] Special issue on Thermoelectric Materials ÑNew Directions and Approaches, T. M. Tritt, M. G. Kanatzidis, H. B. Lyon, G. D. Mahan, Eds., *Mater. Res. Soc. Symp. Proc*. **478** (March 1997).
[8] D.-Y. Chung *et al*., *Mater. Res. Soc. Symp. Proc.* **478**, 333 (1997).
[9] [9]. F. J. DiSalvo, *Science* **285**, 703 (1999); T. M. Tritt, *Science* **283**, 804 (1999).
[10] M. Stordeur, *Phys. Status Solidi* **161**, 831 (1990); H.-H. Jeon, H.-P. Ha, D.-B. Hyun, J.-D. Shim, *J. Phys. Chem. Solids* **4**, 579 (1991); L. R. Testardi, J. N. Bierly Jr., F. J. Donahoe, *J. Phys. Chem. Solids* **23**, 1209 (1962).
[11] W. M. Yim and E. V. Fitzke, *J. Electrochem. Soc.* **115**, 556 (1968); iiii, F. D. Rosi, *J. Mater. Sci.* **1**, 52 (1966); K. Borkowski and J. Przyluski, *Mater. Res. Bull.* **22**, 381 (1987).
[12] W. Jeischko, Metall. Trans. A, 1, 3159 (1970)
[13] Slade R. Culp et al., Appl. Phys. Lett.93, 022105 (2008).
[14] Slade R. Culp et al., Appl. Phys. Lett.88, 042106 (2006).
[15] Su M, Elsbernd CE, Mason T. Jonker "Pear" Analysis of Oxide
[16] Sze, S. M. Physics of Semiconductor Devices 1981, Wiley Inter-Science.
[17] Venkatasubramanian, R. et al. Nature 2001, 413, 597.
[18] W. Jeischko, Metall. Trans. A, 1, 3159 (1970)
[19] Wang Y, Sui Y, Li F, Xu L, Wang X, Su W, et al. Thermoelectrics in misfit-layered oxides [(Ca,Ln)2CoO3]0.62[CoO2]: From bulk to nano. Nano Energy 2012; 1:456–65.